# Flow rate optimization in run-around heat recovery systems

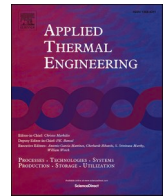N.B. When citing this work, cite the original published paper.

(article starts on next page)

# Flow rate optimization in run-around heat recovery systems

Mohammad Mahmoud [a],[*], Peter Filipsson [a],[b], Samuel Brunninge [c], Jan-Olof Dalenbäck [a]

[a] *Division of Building Services Engineering, Department of Architecture and Civil Engineering, Chalmers University of Technology, 412 96 Gothenburg, Sweden*
[b] *CIT Energy Management AB, 412 88 Gothenburg, Sweden*
[c] *FläktGroup Sweden AB, 553 02 Jönköping, Sweden*

## ABSTRACT

Heat recovery technologies are used to reduce the energy use and the operating costs for ventilation systems in buildings. Run-around heat recovery systems for ventilation are commonly used in buildings when cross-contamination between the air streams is not acceptable, in buildings with complex ducting and in retrofit projects with space limitations. The design and operation of run-around systems are rather complex, especially in ventilation systems with variable air flow rates since the coupling liquid flow rate must be adjusted with respect to the air flow rate.

This paper presents a mathematical model of a run-around heat recovery system. The model is validated with lab measurements and used further in parametric studies to evaluate how the overall thermal effectiveness of a system is influenced by different heat exchanger configurations, coupling liquids and operating conditions. Important findings suggests that the thermal effectiveness is highly sensitive to the coupling liquid flow rate, particularly for systems designed for high thermal effectiveness and for variable air volumes. The optimum liquid flow rate cannot only be determined by the air flow rate as it is influenced by the heat exchanger configuration and the liquid properties and not always found within the turbulent flow regime.

## 1. Introduction

Buildings accounted for 30% of final energy use in 2019, and were responsible for 28% of global carbon dioxide emissions in 2019 [1,2]. The largest share of the carbon dioxide emissions from buildings can be attributed to space heating, accounting for 12% of the total energy use and carbon emissions globally in 2019 [3]. Space heating, including ventilation, is necessary to ensure that a suitable indoor thermal climate and air quality can be maintained.

Different heat recovery technologies are used to decrease the energy use of buildings' ventilation systems. In air-to-air heat recovery systems, the energy from the extract air is recovered and supplied to the fresh supply air. Almost 30% of the energy used in buildings is found in the buildings' extract air [4]. Technologies that adjust air flow rates such as variable-air-volume (VAV) systems have been installed in many buildings to reduce energy use in buildings. Due to the coronavirus outbreak, measures such as increased air flow rates and operating time have been proposed by various HVAC organizations, which will increase energy use in ventilation systems [4,5].

One of the most common heat recovery technologies is the run-around heat recovery system, consisting of two fin-and-tube heat exchangers (coils), connected by a coupling fluid and a pump, as presented in Fig. 1. The coils are placed in the supply and exhaust air handling units. The coupling liquid (usually a mixture of water and an anti-freeze agent such as ethylene glycol) recovers heat from the exhaust air to the supply air. Due to the use of a coupling liquid, the extract air and fresh supply air never pass through the same component. Since the two air streams can be completely separated, run-around heat recovery systems are widely used in buildings with complicated duct systems and when the risk of cross-contamination is not acceptable. These systems have also been implemented in retrofit projects for practical reasons, where the air handling units can be placed in different places in the building.

BELOK, a business network, including some of the largest real estate owners in Sweden, covering approximately 25% of total real estate in Sweden, conducted a survey on run-around heat recovery systems. An important finding reported was that heat recovery efficiency is lower than expected, particularly for systems designed for high efficiency and for systems with variable air flow rates [6]. In the Eco-design directive from the European Union, the minimum allowed effectiveness for run-around heat recovery systems to be sold after 2018 is 68% [7]. A review article about heat recovery technologies for building applications from 2012 states that the effectiveness for existing run-around heat recovery systems typically falls between 45 and 65% [8]. Thus, there is a need to study the systems during different operating conditions and design parameters to achieve high effectiveness.

**Nomenclature**

| | | | |
|---|---|---|---|
| A | Area $[m^2]$ | T | Temperature [K] |
| $c_p$ | Specific heat capacity [J/kgK] | u | Fluid velocity $[m/s]$ |
| C | Capacity flow rate $[W/K]$ | U | Overall heat transfer coefficient $[W/m^2K]$ |
| $C_r$ | Capacity flow ratio [-] | $\dot{V}$ | Volumetric flow $[m^3/s]$ |
| d | Diameter [m] | $X_f$ | Projected fin pattern length for half of one wave [m] |
| $D_c$ | Fin collar outside diameter [m] | $X_L$ | Geometric tube parameter [m] |
| $D_{coil}$ | Depth of coil [m] | $X_M$ | Geometric tube parameter [m] |
| f | Fanning friction factor [-] | | |
| $F_p$ | Fin pitch [m] | *Greek* | |
| h | Convective heat transfer coefficient $[W/m^2K]$ | $\varepsilon$ | Effectiveness [-] |
| j | Colburn factor [-] | $\delta_f$ | Fin thickness [m] |
| k | Thermal conductivity [W/mK] | $\eta_f$ | Fin efficiency [-] |
| l | Pipe length [m] | $\eta_o$ | Surface efficiency [-] |
| $l_{ent.hy}$ | Hydrodynamic entrance length [m] | $\nu$ | Kinematic viscosity $[m^2/s]$ |
| $l_{ent.th}$ | Thermal entrance length [m] | $\rho$ | Density $[kg/m^3]$ |
| L | Total tube length [m] | | |
| N | Number of tube rows [-] | *Subscripts* | |
| NTU | Number of transfer units [-] | a | Air side |
| Nu | Nusselt number [-] | c | Cold side |
| p | Pressure [Pa] | f | Fin |
| Pr | Prandtl number [-] | h | Hot side |
| $P_d$ | Fin waffle height [m] | H | Hydraulic |
| $P_l$ | Longitudinal tube pitch [m] | i | Internal |
| $P_t$ | Transverse tube pitch [m] | l | Liquid side |
| q | Recovered heat transfer rate [W] | m | mean |
| $\dot{Q}$ | Heat transfer rate [W] | max | Maximum, theoretically |
| r | Tube internal radius [m] | min | Minimum |
| $R_{eq}$ | Equivalent radius for circular fin [m] | o | Outside, overall |
| Re | Reynolds number [-] | t | Tube |
| | | tot | Total |
| | | UHF | Uniform heat flux |
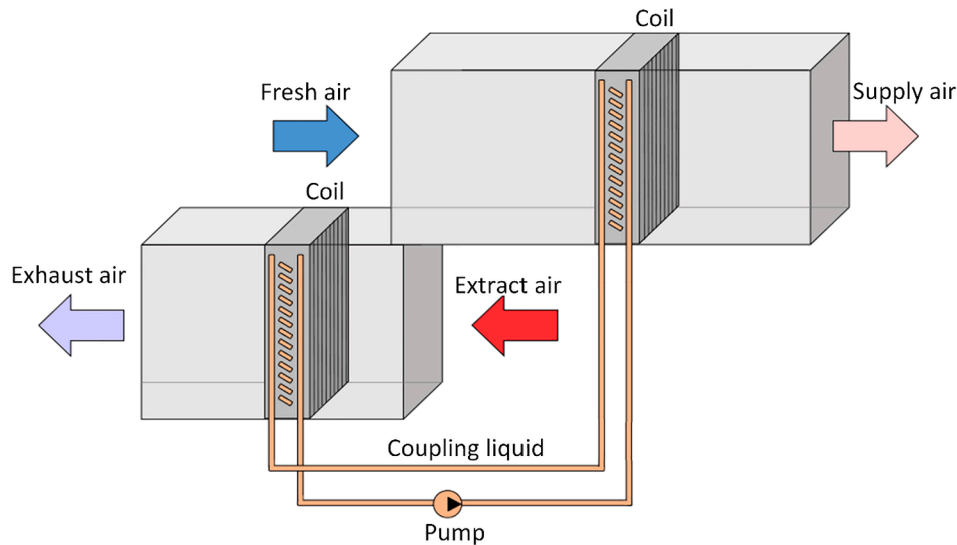


**Fig. 1.** A schematic of a run-around heat recovery system.

*1.1. Previous studies on run-around heat recovery systems*

Kays & London [9] presented the theory for run-around heat recovery systems and showed that the overall effectiveness of a system using two coils and a coupling liquid can be determined by determining the effectiveness of each one of the coils, the hot and cold fluid capacity rates and the coupling liquids' capacity rate. The authors could show

that a system with equal hot and cold fluid capacity flow rates will have a maximum overall effectiveness when the capacity rate of the coupling fluid is equal to the capacity flow rate of the air streams.

Holmberg [10] further developed the work of Kays & London [9] by deriving an expression for the optimum coupling liquid capacity flow rate for a run-around heat recovery system. The liquid velocity was treated as independent of the coupling liquid flow rate, concluding that

maximum effectiveness was achieved when the capacity flow rate of the liquid was equal to the capacity flow rate of the air. Holmberg [10] showed that systems designed for high overall effectiveness are more sensitive to the coupling fluid capacity rate.

Forsyth & Besant [11] studied how some of the coil parameters affect the overall effectiveness for a run-around heat recovery system. The authors developed a mathematical model describing a system, in which a sensitivity analysis of various heat exchanger configuration parameters were analyzed. The accuracy of the model and how representative the model is for real systems is uncertain. The model could not be verified due to significant differences between the modelled coils and the real coils in a system from which data was acquired through field measurements. By means of various calculations, the authors could conclude that the effectiveness of the system was mostly sensitive to changes of the liquid flow rate and tube diameter, and was least sensitive to fin spacing and fin thickness. Data from the field measurements showed that the maximum effectiveness was not found at a capacity flow ratio of unity.

Forsyth & Besant [12] showed that the assumption of using a steady-state model to analyze run-around heat recovery systems is justified since the changes in temperatures within the system are much faster than the changes of the ambient conditions. The Forsyth & Besant [12] study compared the theoretical model presented by Kays & London [9] with measured data, and concluded that the error was well within ±5%. The authors concluded that turbulent flow on the tube side of the coils is essential to achieve a high overall effectiveness.

Zeng et al. [13] concluded that it is important to include the effect of temperature-dependent properties for the coupling liquid when modelling run-around heat recovery systems. The model was established by dividing the heat exchanger into several elements and analyzing the temperature variations along the tubes in the coil. Using temperature-independent properties for the coupling-liquid, especially for pure water, can greatly influence the results because the viscosity can change rapidly due to temperature changes. Using an equal mixture of water and ethylene glycol dramatically reduced the predicted error. Calculating the coupling liquids properties at an average temperature increases the error for cases with large temperature differences, high glycol concentrations and for Reynolds numbers between 2 500 and 5 000.

Balen et al. [14] developed a mathematical model and conducted experimental measurements in a rig for two different types of coils with different fin pitches and fin thicknesses. Pure water was used as the coupling liquid and the outdoor temperature was in the range of 13.8 – 52.0 °C. The authors reported that the deviation in most cases was ±3%. The authors concluded that the fluid temperatures did not affect the overall thermal effectiveness, which contradicts Zeng et al.'s findings [13]. For both coil types, the maximum effectiveness for the system was found at a capacity flow ratio of unity, which is aligned with the theory presented by both Kays & London [9] and Holmberg [10].

Besides the above articles focusing on more traditional run-around heat recovery systems using coils there is also published research related to other configurations, for example using flat-plate heat exchangers instead of coils and including a heat pump in the system.

Fan et al. [15] studied run-around heat recovery systems using flat-plate heat exchangers instead of coils, showing that for cross-flow configuration the optimum overall effectiveness is found when the capacity flow ratio ranges between 0.8 and 1.2. Vali et al. [16] established correlations for counter/cross flow flat-plate heat exchangers based on the entrance ratio and aspect ratio for the heat exchanger. The correlations were used to predict the sensible overall effectiveness for run-around heat recovery systems and the authors could show that the NTU for the heat exchangers should be larger than 3 and the capacity flow ratio should be in the range of 0.8–1.2, which is well aligned with the Fan et al. [15] findings.

Wallin et al. [17] summarizes findings from previous studies examining how the annual energy performance for run-around heat recovery systems are affected by including a heat pump. One of the findings reported suggests that the annual heat recovery rate for a modelled system in Stockholm would increase from 47% to 65% using a three-stage heat pump compared to a conventional run-around heat recovery system.

No previous study has used a validated model to study whether the optimum capacity flow ratio is affected by the coupling liquid mixture, i. e. the water and glycol concentration. Also, no previous study has shown how the effectiveness is altered for VAV systems using a water and ethylene glycol mixture as the coupling liquid in a verified model, including the laminar flow regime on the liquid side using coils.

### 1.2. Objectives

The objectives of this study are to develop and validate a model for sensible heat recovery using coils in a run-around heat recovery system. The aim is to determine the effect of the coupling liquid flow rate on the thermal effectiveness at different air flow rates and the effect of ethylene glycol concentration and circuitry arrangement on the results. Finally, the model aims to investigate the influence of variable air flow volumes on the effectiveness of a run-around heat recovery system. In the model, calculations should be conducted for cases with both laminar and turbulent flow on the liquid side, different ethylene glycol concentration and coupling liquid velocities.

## 2. Method

The method comprises literature studies, model development and model validation. The effectiveness of the coils used in the study was found by mathematically describing the coil configuration using correlations for heat transfer and pressure drop. The effectiveness of the system was calculated using the theories presented by Kays & London [9] and Holmberg [10]. The fin geometry was hard to measure and could not be acquired from the manufacturer due to intellectual property rights. To verify the established model with the assumptions made, the pressure drop was also modelled to allow for an evaluation of two parameters. The modelled effectiveness and pressure drop of the system were compared to data acquired from measurements conducted in a test rig to validate the model. The test rig complied with the European standard EN-308, describing the test procedures for establishing the performance of air-to-air heat recovery systems.

### 2.1. Model

The modelled run-around heat recovery system consists of two coils, two air streams and a coupling liquid. Only the inlet temperatures and flow rates of the two air streams are known, thus it is not possible to
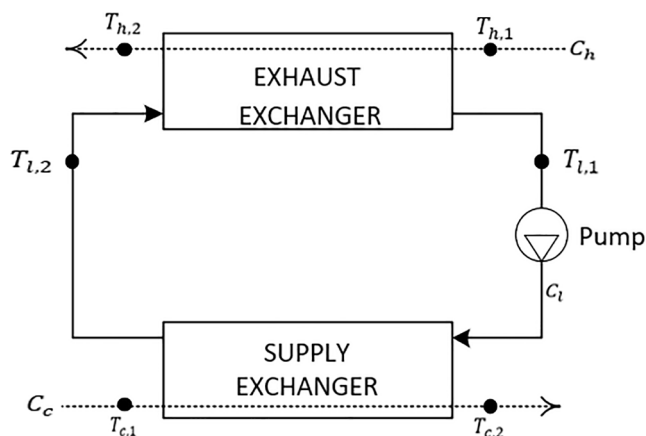
**Fig. 2.** Schematic diagram of the heat recovery system showing temperatures and capacity flow rates.

calculate energy recovery by simple energy balances. The effectiveness-NTU method was used to find the outlet temperatures for the two air streams and the temperatures of the coupling liquid. The effectiveness of a heat exchanger can be expressed by [Eq. (1)].

$$\varepsilon = f(NTU, C_r, flow\ arrangement) \tag{1}$$

The effectiveness of a heat exchanger is defined in [Eq. (2)] as the ratio between the recovered energy q and the theoretically maximum heat recovery $q_{max}$.

$$\varepsilon = \frac{q}{q_{max}} \tag{2}$$

The capacity flow rate C for each stream in a heat exchanger is defined as the product of the volumetric flow $\dot{V}$, the density $\rho$ and the specific heat capacity $c_p$ given by [Eq. (3)] and presented in Fig. 2.

$$C = \dot{V} \rho c_p \tag{3}$$

The smaller capacity flow rate is defined as $C_{min}$ and the larger as $C_{max}$. The capacity flow ratio $C_r$ is given by [Eq. (4)].

$$C_r = \frac{C_{min}}{C_{max}} \tag{4}$$

The UA value is defined as the heat exchangers' overall thermal conductance, which is the product of the overall heat transfer coefficient U and the heat transfer area A. The number of transfer units, NTU, is defined in [Eq. (5)], where $C_{min}$ is the smallest capacity flow rate of the two streams being heat exchanged.

$$NTU = \frac{UA}{C_{min}} \tag{5}$$

For different heat exchanger flow arrangements it is possible to derive functions expressing the effectiveness as a function of NTU and $C_r$ as presented in [Eq. (1)] [18]. In the model, a counterflow arrangement is assumed due to the use of many tube rows in the coil [14] and few circuits, making it possible to determine the effectiveness from [Eq. (6)]

$$\varepsilon = \frac{1 - \exp[-NTU(1 - C_r)]}{1 - C_r \exp[-NTU(1 - C_r)]} \tag{6}$$

The overall conductance for a fin-and-tube heat exchanger is given by [Eq. (7)], where $h_l$ is the convective heat transfer coefficient on the liquid side, $A_l$ is the heat transfer area on the liquid side, $d_o$ is the outside tube diameter, $d_i$ is the internal tube diameter, $k_t$ is the thermal conductivity of the tube material, L is the total tube length, $\eta_o$ is the surface efficiency, $A_a$ is the heat transfer area on the air side and $h_a$ is the convective heat transfer coefficient on the air side.

$$\frac{1}{UA} = \frac{1}{(h_l A_l)_l} + \frac{\ln(d_o/d_i)}{2\pi k_t L} + \frac{1}{(\eta_o A_a h_a)_a} \tag{7}$$

The convective heat transfer coefficients of the liquid side $h_l$, and air side $h_a$, must be found in order to determine the UA value. These depend on the velocity and the coil configuration and cannot usually be solved analytically. To find the coefficients, numerical methods and empirical relationships are used. These are described below.

The thermophysical properties of the air and coupling liquid (the water and ethylene glycol mixture) were calculated using correlations published in [19–25]. All fluid properties were calculated at the average temperature of the fluid's inlet and outlet temperatures.

### 2.1.1. Liquid side

The Reynolds' number for internal flow through a tube is defined by [Eq. (8)], where $u_m$ is the average fluid velocity, $d_i$ is the internal tube diameter and $\nu$ is the kinematic viscosity of the fluid.

$$Re = \frac{u_m d_i}{\nu} \tag{8}$$

For $Re < 2300$ the fluid is assumed to be within the laminar flow

regime for internal flow [18]. The flow can be characterized as developing flow or a fully developed flow depending on the thickness of the hydrodynamic and thermal boundary layers. Since the coupling liquid was a water and ethylene glycol mixture with high viscosity, i.e. with a Prandtl-number $\gg$ 1, the thermal entrance length was longer than the hydrodynamic entrance length.

For turbulent flow, the hydrodynamic entrance length, $l_{ent,hy}$ is independent of the Reynolds number [26] and is approximated by [Eq. (9)].

$$\frac{l_{ent,hy}}{d_H} \approx 10 \tag{9}$$

Using [Eq. (9)] made it possible to confirm that the hydrodynamic entrance length is short compared to the length of a tube in the heat exchanger. Due to the mixing phenomena that characterize turbulent flow, the thermal boundary layer was assumed to be short relative to the length of a tube in the heat exchanger. The flow was assumed to be fully developed within the turbulent flow regime.

The hydrodynamic and thermal entrance region for laminar flow were approximated using [Eq. (10)] and [Eq. (11)] [26]. For cases where the thermal entrance length was in the same order of magnitude as the length of a tube, the flow was assumed to be developing.

$$\frac{l_{ent,hy}}{d} = \frac{0.60}{0.035Re + 1} + 0.056Re \tag{10}$$

$$\frac{l_{ent,th}}{d} \approx 0.05RePr \tag{11}$$

For viscous liquids with laminar conditions the thermal entrance region is reset after a U-bend in the heat exchanger connecting two tubes, which was shown by Hrnjak & Hong [27] and Stignor et al. [28]. The flow was therefore assumed to re-develop after each U-bend.

To find the convective heat transfer coefficient on the liquid side, $h_l$, correlations were used to find the Nusselt number defined by [Eq. (12)] where $d_i$ is the internal tube diameter and k is the thermal conductivity of the fluid.

$$Nu = \frac{h_l d_i}{k} \tag{12}$$

For a fully-developed turbulent flow, the Nusselt number was calculated by Gnielinski's empirical equation [Eq. (13)], where f is the Fanning friction factor given by [Eq. (14)]. Re is the Reynolds number and $Pr$ is the Prandtl-number [26].

$$Nu = \frac{(f/8)(Re - 1000)Pr}{1 + 12.7(f/8)^{\frac{1}{2}}(Pr^{2/3} - 1)} \tag{13}$$

$$f = (0.790lnRe - 1.64)^{-2} \tag{14}$$

For developing laminar flow assuming uniform wall heat flux, the Nusselt number is calculated using [Eq. (15)], [Eq. (16)], [Eq. (17)] and [Eq. (18)], where $d_i$ is the internal tube diameter, l is the length of the tubes between two U-bends, $Re$ is the Reynolds number and $Pr$ is the Prandtl-number [26].

$$Nu_{UHF} = \left[ Nu_{UHF,1}^3 + 0.6^3 + (Nu_{UHF,2} - 0.6)^3 + Nu_{UHF,3}^3 \right]^{1/3} \tag{15}$$

$$Nu_{UHF,1} = 4.364 \tag{16}$$

$$Nu_{UHF,2} = 1.953 \left( \frac{d_i}{l} \right)^{\frac{1}{3}} (RePr)^{1/3} \tag{17}$$

$$Nu_{UHF,3} = 0.924Pr^{1/3} \left[ \left( \frac{d_i}{l} \right) Re \right]^{1/2} \tag{18}$$

### 2.1.2. Air side

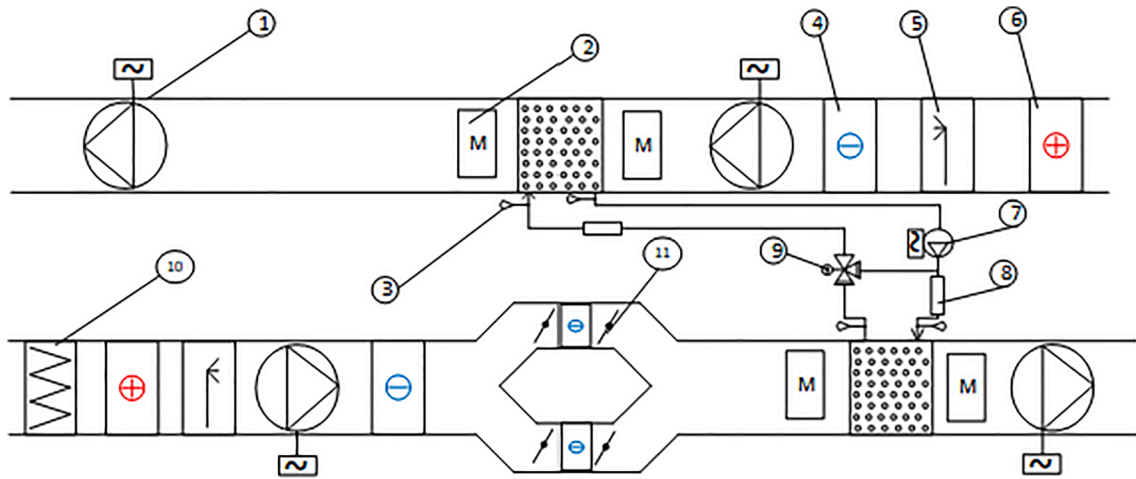The flow characteristics and heat transfer on the air side is complex

**Fig. 3.** Schematic diagram of the rig.

due to the fin-and-tube geometry, which causes drag formation and vortices around the tubes and in between the fins. Due to the complex formation and separation of the boundary layers that depend on the heat exchanger configuration correlations were used to determine the Colburn factor, j, and the Fanning friction factor, f. The correlations used were presented by Wang [29] as [Eq. (19)] and [Eq. (20)]. In the following equations, $Re_{D_c}$ is the Reynolds number based on the outside tube diameter including the fin-collar thickness. $P_l$ is the longitudinal tube pitch, $\delta_f$ is the fin thickness, $F_p$ is the fin pitch, $D_c$ is the fin collar outside diameter, N is the number of tube rows, $P_d$ is the fin waffle height, $X_f$ is the projected fin pattern length for half of one wave, $P_t$ is the transverse tube pitch, $A_{tot}$ is the total heat transfer area, $A_t$ is the external tube surface area, $D_H$ is the hydraulic diameter defined at the minimum free flow area between the tubes and the fin-collar.

The Fanning friction factor found from [Eq. (20)] includes the internal friction, entrance and exit effects [30] making it possible to calculate the total pressure drop using [Eq. (25)] where $\Delta p$ is the pressure drop across the heat exchanger, f is the Fanning friction factor, $D_H$ is the hydraulic diameter defined at the minimum free flow area between the tubes and the fin-collar, $\rho$ is the air density and $u_m$ is the average air velocity at the minimum free flow area.

$$\Delta p = f \frac{4 * D_{coil}}{D_H} \frac{\rho u_m^2}{2} \tag{25}$$

The fin efficiency, $\eta_f$, was calculated by using Schmidts approximation [31] which is quoted in [32,33,34] for staggered tube arrangement as [Eq. (26)]

$$j = 1.79097 Re_{D_c}^{-0.1707 - 1.374\left(P_t/\delta_f\right)^{(-0.493)}\left(F_p/D_c\right)^{-0.886}N^{-0.143}\left(P_d/X_f\right)^{-0.0296}} * \left(\frac{P_l}{\delta_f}\right)^{-0.456} N^{-0.27} \left(\frac{F_p}{D_c}\right)^{-1.343} \left(\frac{P_d}{X_f}\right)^{0.317} \tag{19}$$

$$\eta_f = \frac{\tanh(mr\varnothing)}{mr\varnothing} \tag{26}$$

where m and $\varnothing$ are found from [Eqs. (27)–(31)], $h_a$ is the air side heat transfer coefficient, r is the tube internal radius, $k_f$ is the thermal conductivity of the fin material, $\delta_f$ is the fin thickness, $P_t$ is the transverse tube pitch and $P_l$ is the longitudinal tube pitch.

$$f = 0.05273 Re_{D_c}^{f_1} \left(\frac{F_p}{X_f}\right)^{f_2} \left(\frac{F_p}{P_t}\right)^{f_3} \left[\ln\left(\frac{A_{tot}}{A_t}\right)\right]^{-2.726} \left(\frac{D_H}{D_c}\right)^{0.1325} N^{0.02305} \tag{20}$$

Coefficients $f_1$, $f_2$ and $f_3$ are found from [Eq. (21)], [Eq. (22)] and [Eq. (23)]

$$m = \sqrt{\frac{2h_a}{k_f \delta_f}} \tag{27}$$

$$f_1 = 0.1714 - 0.07372 \left(\frac{F_p}{P_l}\right)^{0.25} \ln\left(\frac{A_{tot}}{A_t}\right) \left(\frac{P_d}{X_f}\right)^{-0.2} \tag{21}$$

$$\varnothing = \left(\frac{R_{eq}}{r} - 1\right)\left[1 + 0.35\ln\left(R_{eq}/r\right)\right] \tag{28}$$

$$f_2 = 0.426 \left(\frac{F_p}{P_t}\right)^{0.3} \ln\left(\frac{A_{tot}}{A_t}\right) \tag{22}$$

$$\frac{R_{eq}}{r} = 1.27 \frac{X_M}{r} \left(\frac{X_L}{X_M} - 0.3\right)^{0.5} \tag{29}$$

$$f_3 = \frac{-10.2192}{\ln(Re_{D_c})} \tag{23}$$

$$X_L = \sqrt{(P_t/2)^2 + (P_l^2/2)} \tag{30}$$

Since the Colburn factor is found from [Eq. (19)], it is possible to determine the Nusselt number by [Eq. (24)], and further determine the $h_a$, the convective heat transfer coefficient on the air side, by using [Eq. (12)].

$$X_M = \frac{P_t}{2} \tag{31}$$

$$\mathrm{Nu} = j Re_{D_c} Pr^{1/3} \tag{24}$$

Surface efficiency, $\eta_o$, was calculated using [Eq. (32)], where $A_{tot}$ is

the total heat transfer surface area on the air side, $A_f$ is the finned surface area and $\eta_f$ is the fin efficiency calculated from [Eq. (26)].

$$\eta_o = 1 - \frac{A_f}{A_{tot}}(1 - \eta_f) \tag{32}$$

### 2.1.3. Overall effectiveness

The heat exchangers' overall thermal conductance, UA, was determined for each coil using [Eq. (7)]. Since all capacity flow rates were known, it was possible to determine the capacity flow ratio by [Eq. (4)] and thus also determine the NTU from [Eq. (5)], in turn making it possible to determine the effectiveness for each coil from [Eq. (6)]. Holmberg [10] presented [Eq. (33)] from which it is possible to determine the overall effectiveness of the system, $\varepsilon_o$. In [Eq. (33)] $C_{min,o}$ is the overall minimum capacity flow rate, $C_{min,h}$ is the smallest of the two capacity flow rates through the coil on the exhaust side, $\varepsilon_h$ is the effectiveness of the coil on the exhaust side, $\varepsilon_c$ is the effectiveness of the coil on the supply side, $C_{min,c}$ is the smallest of the two capacity flow rates through the coil on the supply side and $C_l$ is the capacity flow rate of the coupling liquid.

$$\varepsilon_o = \frac{1}{\frac{C_{min,o}/C_{min,h}}{\varepsilon_h} + \frac{C_{min,o}/C_{min,c}}{\varepsilon_c} - \frac{C_{min,o}}{C_l}} \tag{33}$$

Also, since the effectiveness of each coil was found, the four unknown temperatures in the system $T_{h,2}, T_{c,2}, T_{l,1}$ and $T_{l,2}$ (see Fig. 2) could be determined. To validate whether the found solution satisfies the laws of thermodynamics, an energy balance was conducted for the two coils by [Eq. (34)], [Eq. (35)] and [Eq. (36)].

$$\dot{Q}_h = C_h(T_{h,1} - T_{h,2}) \tag{34}$$

$$\dot{Q}_c = C_C(T_{c,2} - T_{c,1}) \tag{35}$$

$$\dot{Q}_l = C_l(T_{l,1} - T_{l,2}) \tag{36}$$

The modelling required iterations due to temperature dependent fluid properties. The iterations continued until the difference between the calculated powers in [Eq. (34)], [Eq. (35)] and [Eq. (36)] were smaller than 0.01 %.

### 2.2. Measurements

A schematic diagram of the rig setup is shown in Fig. 3. Measurements were conducted in a rig in accordance with the European standard EN 308 in order to evaluate the overall effectiveness of the run-around heat recovery system for various air flow rates, coupling liquid flow rates, outdoor air temperatures and extract air temperatures.

A water and ethylene glycol mixture 37% (weight) was used as the coupling liquid. The two coils were of the fin-and-tube type with wavy aluminum fins, having a finned width of 1150 mm, a height of 603 mm, a depth of 330 mm, 2 mm fin-pitch, copper tubes with an outside diameter of 12 mm, 19 tubes in the transverse direction, 12 tube-rows in the air direction and with four circuits for the coupling liquid.

The fans (1) were frequency-controlled, which allowed for changes in the air flow rate. In the measuring positions (2) before and after each coil, the pressure drop was measured using pressure transmitters of type PSIDAC 6280 with an uncertainty of ±0.5%. Temperature sensors of type PT-1000 calibrated against water at the triple point with an uncertainty of ±0.05K were used to measure the air temperature across the cross section. The relative humidity sensors were calibrated against a chilled mirror dew point hygrometer with an uncertainty from the dewpoint of ±0.16K. The air flow rate was determined by measuring the pressure difference over a nozzle. Thermocouples (3) were used to measure the coupling liquid temperature into and out of each coil. Cooling coils (4), humidifiers (5) and heating coils (6) were used to achieve the desired temperature and humidity testing conditions. The
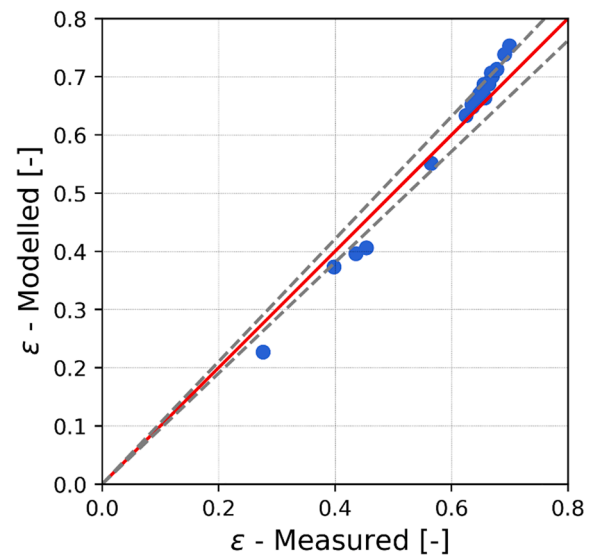


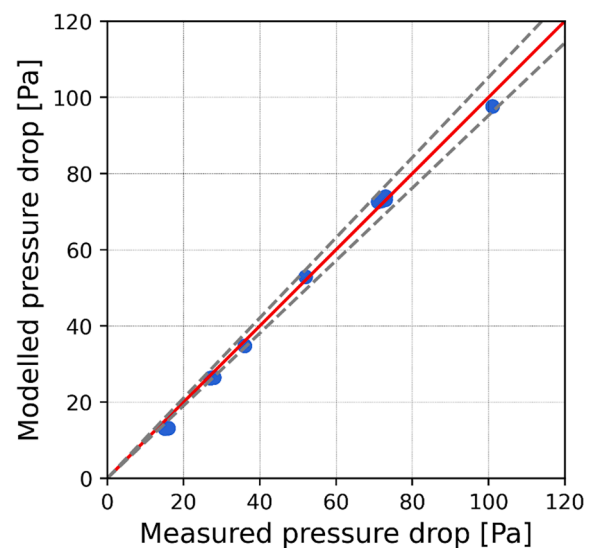**Fig. 4.** The modelled and measured effectiveness.



**Fig. 5.** The modelled and measured pressure drop.

coupling liquid was pumped by a frequency-controlled pump (7) which allowed for changes in liquid flow rate, the flow was measured using a magnetic inductive flow meter (8) with an uncertainty of ±0.5%. In the coupling circuit, a fully open control valve (9) was located. The outdoor air passed a filter (10) and the air flow was cooled and dehumidified by using one or two of the secondary cooling coils by controlling the dampers (11).

The tests were conducted for 21 different operating conditions with balanced air flows rates in the range of $0.3 – 1.2 \ m^3/s$. The coupling liquid flow rate correspondingly varied in the range of 0.031 l/s and 0.396 l/s in order to evaluate the effectiveness at different capacity flow ratios. Outdoor air temperature was changed in the range of $-5.5 \ ^{\circ}C – 5.2 \ ^{\circ}C$ with a relative humidity between 57% and 88%. Extract air temperature was changed in the range of $19.9 \ ^{\circ}C – 25.1 \ ^{\circ}C$ with a relative humidity between 9% and 33%. The absolute humidity of the extract air stream was calculated to ensure that no condensation occurred. For each change of any parameter the rig was run for at least one hour, allowing for steady state conditions to settle before the collection of any measuring data. The sensors in the rig were connected to LabVIEW, where the data from the tests were gathered.
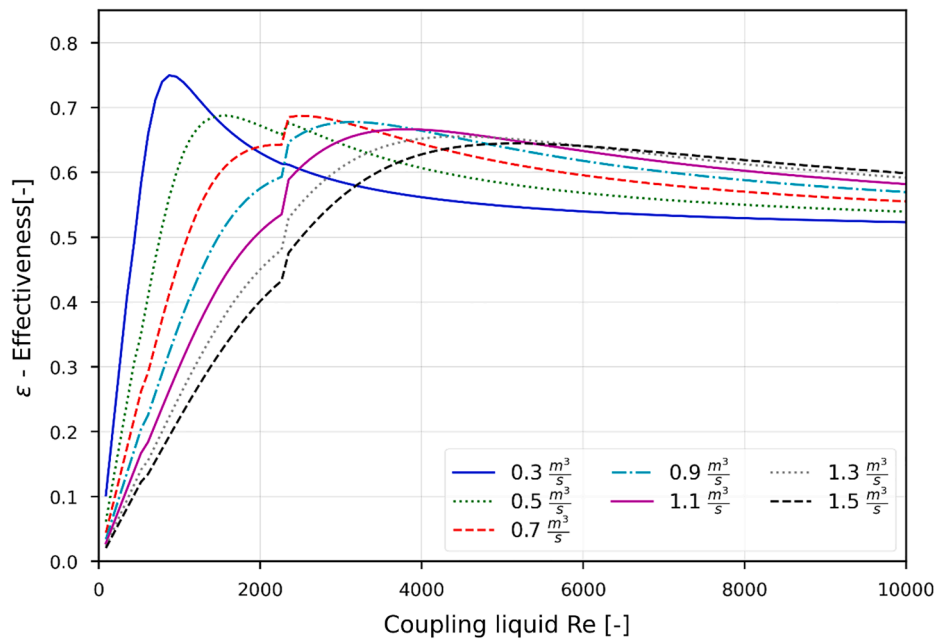
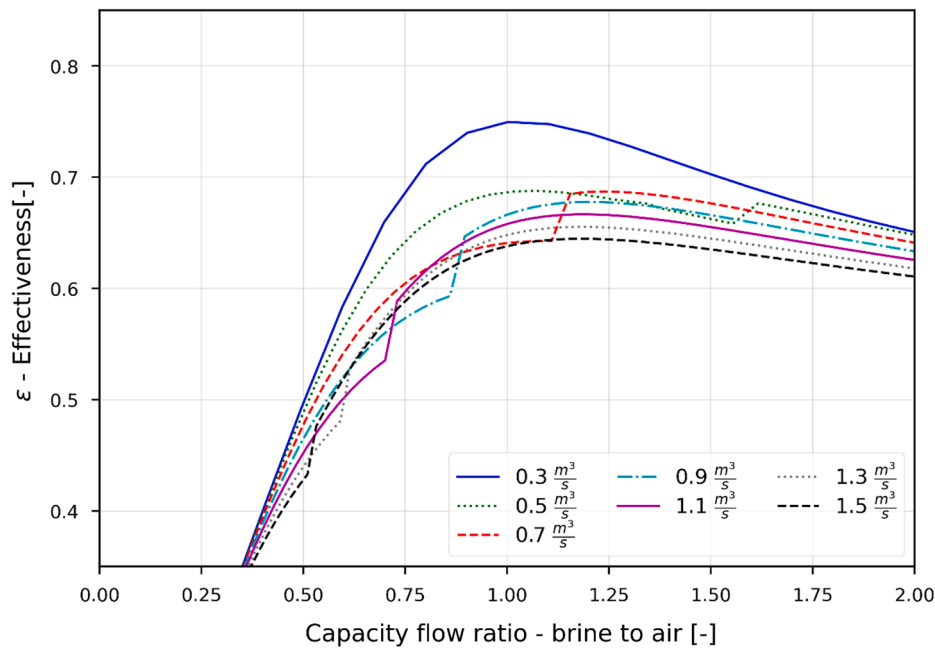**Fig. 6.** The effectiveness related to the coupling liquid Reynolds number with 37% ethylene glycol.



**Fig. 7.** The effectiveness at different air flow rates and capacity flow ratios with 37% ethylene glycol.

Based on the sensor uncertainties the uncertainty of the measured effectiveness is estimated to 0.0029 – 0.0044.

## 3. Results

### 3.1. Model validation

The established mathematical model of the system was evaluated by comparing the measured and modelled effectiveness and the pressure drop across the coils. The measured and modelled effectiveness is presented in Fig. 4. The dashed lines show a deviation of ±5%. The mean absolute deviation was 0.028, the root mean square error was 0.031, with a maximum deviation of 0.054.

The measured and modelled pressure drop across the supply-side coil is presented Fig. 5. The dashed lines show a deviation of ±5%. The mean absolute deviation is 1.51 Pa, the root mean square error is 1.70 Pa with a maximum deviation of 3.34 Pa.

### 3.2. Modelling

Effectiveness was modelled for air flow rates in the range of $0.3 – 1.5$ $m^3/s$ at an outdoor temperature of $0\,°C$ and an extract air temperature of $20\,°C$. The air flow rate was extrapolated outside the testing range, where the maximum air flow rate was $1.2\ m^3/s$.
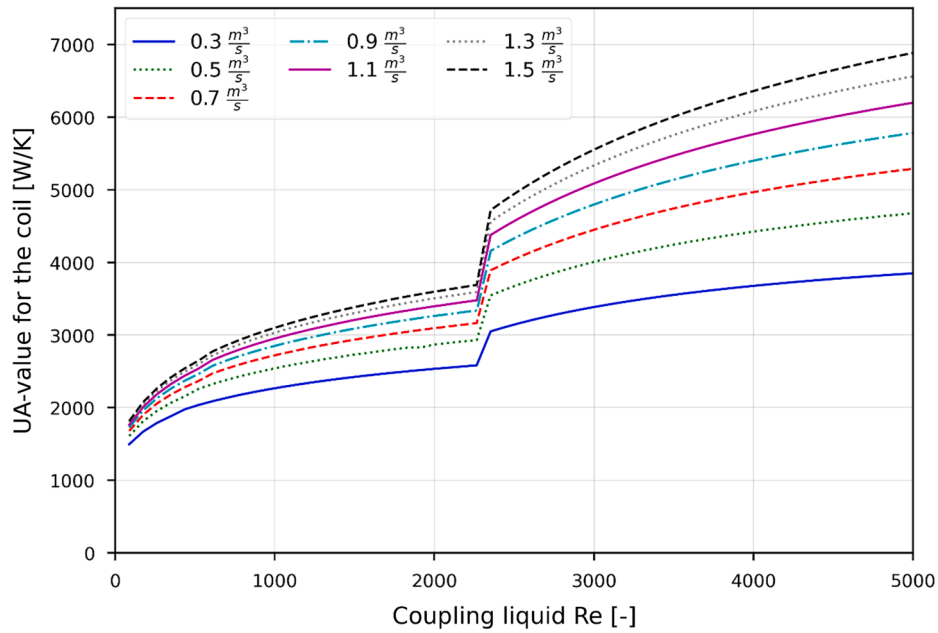
**Fig. 8.** The UA-value for the coil at different air flow rates and Reynolds number with 37% ethylene glycol.

**Table 1**
The maximum effectiveness for each air flow rate and ethylene glycol concentration.

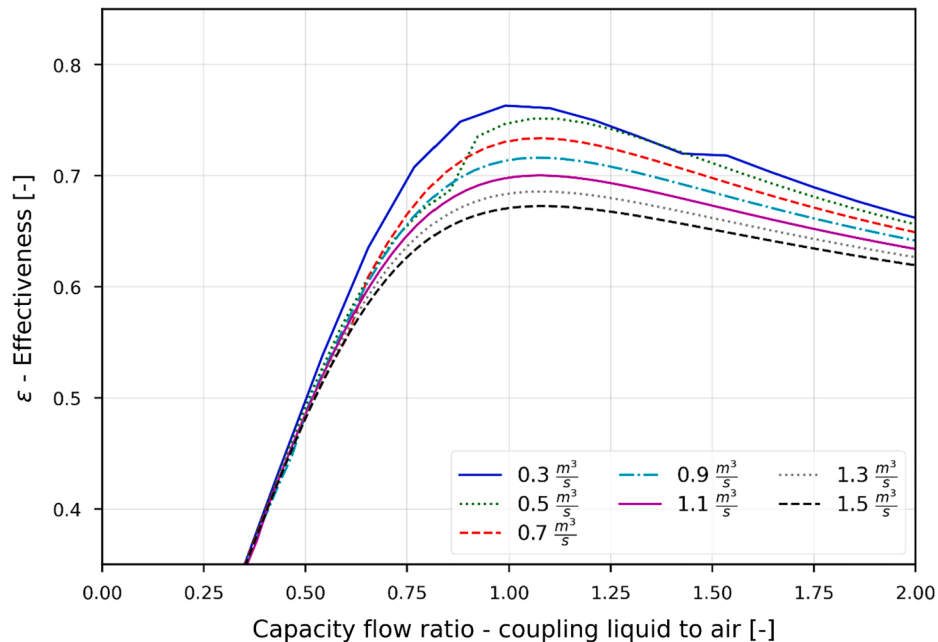| Glyc. Conc. | Air flow rate | | | | | | |
|---|---|---|---|---|---|---|---|
| | $0.3 \left[\frac{m^3}{s}\right]$ | $0.5 \left[\frac{m^3}{s}\right]$ | $0.7 \left[\frac{m^3}{s}\right]$ | $0.9 \left[\frac{m^3}{s}\right]$ | $1.1 \left[\frac{m^3}{s}\right]$ | $1.3 \left[\frac{m^3}{s}\right]$ | $1.5 \left[\frac{m^3}{s}\right]$ |
| 10 % | 0.763 | 0.751 | 0.734 | 0.716 | 0.700 | 0.686 | 0.673 |
| 20 % | 0.758 | 0.733 | 0.720 | 0.705 | 0.690 | 0.676 | 0.664 |
| 30 % | 0.754 | 0.701 | 0.702 | 0.690 | 0.677 | 0.665 | 0.653 |
| 40 % | 0.747 | 0.686 | 0.680 | 0.672 | 0.661 | 0.651 | 0.640 |



**Fig. 9.** The effectiveness for different air flow rates and capacity flow ratios with 10 % ethylene glycol.

### 3.2.1. Variable air volume

In the modelling for variable air volumes, the coupling liquid had an ethylene glycol concentration of 37%. The effectiveness for the different air flow rates and the coupling liquid Reynolds number (which increases proportionally with the coupling liquid flow rate) is presented in Fig. 6. The modelling demonstrates that the maximum achievable effectiveness
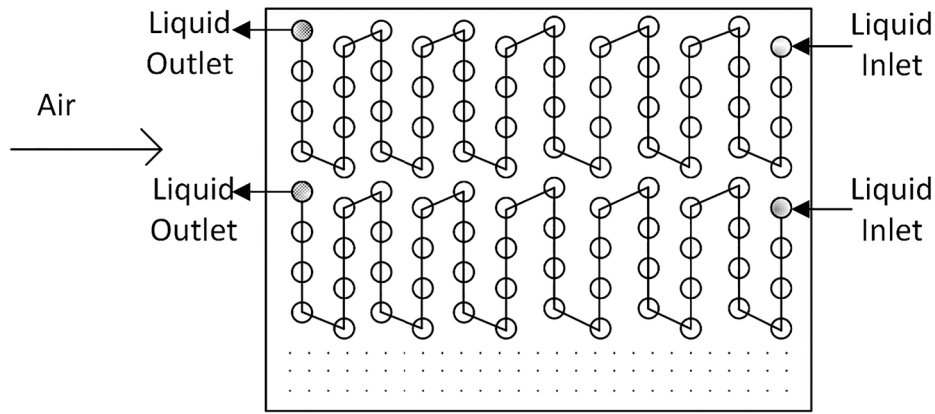
**Fig. 10.** Schematic diagram showing the number of circuits and the number of tube rows.

**Table 2**
The maximum effectiveness for each air flow rate and number of circuits.

| # circuits | Air flow rate | | | | | | |
|---|---|---|---|---|---|---|---|
| | $0.3 \left[\frac{m^3}{s}\right]$ | $0.5 \left[\frac{m^3}{s}\right]$ | $0.7 \left[\frac{m^3}{s}\right]$ | $0.9 \left[\frac{m^3}{s}\right]$ | $1.1 \left[\frac{m^3}{s}\right]$ | $1.3 \left[\frac{m^3}{s}\right]$ | $1.5 \left[\frac{m^3}{s}\right]$ |
| 1 | 0.827 | 0.795 | 0.770 | 0.748 | 0.730 | 0.714 | 0.700 |
| 2 | 0.770 | 0.763 | 0.743 | 0.725 | 0.708 | 0.694 | 0.680 |
| 3 | 0.758 | 0.726 | 0.715 | 0.701 | 0.687 | 0.674 | 0.662 |
| 4 (real) | 0.750 | 0.688 | 0.687 | 0.677 | 0.667 | 0.655 | 0.645 |

decreases with an increased air flow rate. For cases with an air flow rate of 0.3 and 0.5 $m^3/s$ the maximum effectiveness was found within the laminar flow regime at the liquid side. There is an optimum effectiveness for each air flow rate, which is more distinctive for cases with lower air flow rates.

In Fig. 7, effectiveness is presented with respect to the capacity flow ratio. The modelling clearly shows that maximum effectiveness is found at different capacity flow ratios for the different air flow rates.

In Fig. 8, the overall thermal conductance for the coil, the UA-value, is shown for the different air flow rates and the coupling liquid's Reynolds number. The coils' UA-value increases with increasing coupling

liquid Reynolds number, and a significant increase is found at a Reynolds number of 2 300, because the liquid flow leaves the laminar flow regime.

### 3.2.2. Influence of glycol concentration

The effectiveness for the system was modelled with different ethylene glycol concentration in the coupling liquid for different air flow rates. Table 1 presents the maximum effectiveness for each air flow rate with different ethylene glycol concentrations. The modelling clearly demonstrates that the maximum effectiveness found for each air flow rate decreases with an increased ethylene glycol concentration. The
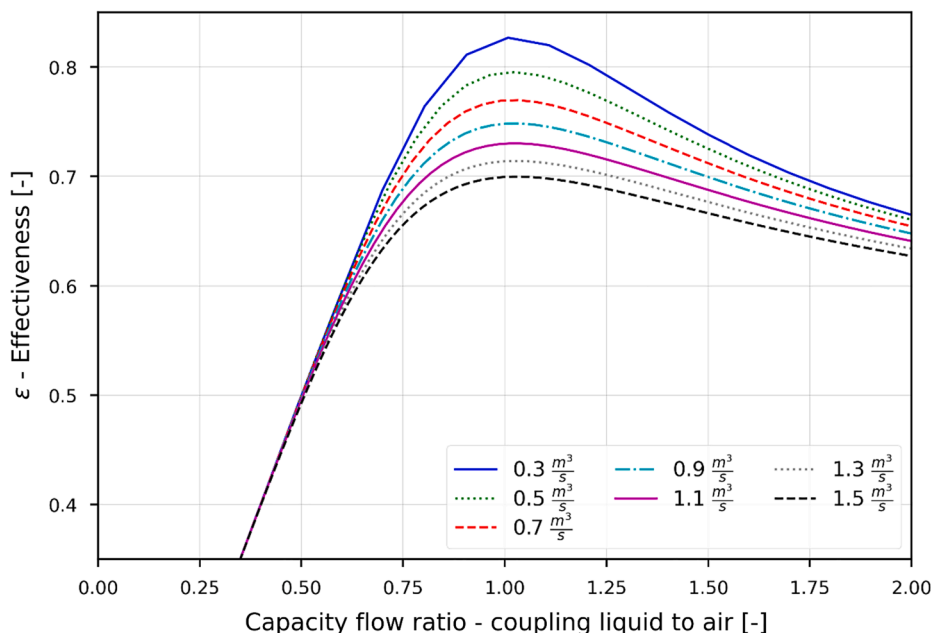


**Fig. 11.** The effectiveness for one coupling liquid circuit with 37% ethylene glycol.

results also shows that the decrease in effectiveness is more prominent for certain air flow rates, which can be seen by comparing the air flow rate of $0.5 \frac{m^3}{s}$ to the air flow rates of $0.3 \frac{m^3}{s}$ and $1.5 \frac{m^3}{s}$. For the case with an ethylene glycol concentration of 10%, (see Fig. 9), the characteristics of the effectiveness to the capacity flow ratio are notably different compared to Fig. 7. The change in effectiveness varies in a smoother manner with the capacity flow ratio and maximum effectiveness is found at a capacity flow ratio closer to unity for all air flow rates. In Appendix A, Figs. A1–A4 show how variations in the ethylene glycol concentration in the range of 10–40% affected effectiveness with respect to the capacity flow ratio. With an increased ethylene glycol concentration, Figs. A1–A4 clearly show how the highest effectiveness is found at different capacity flow ratios further away from unity. The increase in ethylene glycol concentrations to 30% and 40% clearly show that the transition out of the laminar flow regime becomes more prominent for effectiveness.

### 3.2.3. Influence of the coupling liquid velocity

The influence of different coupling liquid velocities was studied using 37 % ethylene glycol. The velocity of the coupling liquid depends on the flow rate, the internal tube diameter, and the number of circuits. A change in tube diameter would change the coil configuration, and thus the heat transfer on the air side. To evaluate how the coupling liquid velocity affects the effectiveness for different air flow rates, the number of circuits in the coils is reduced, keeping everything constant on the air side. For example, a coil with two circuits is presented in Fig. 10, i.e. the number of circuits is determined from the number of coupling liquid inlets from the header through the coil.

The reduction in the number of circuits reduces the coupling liquid flow area, achieving a higher velocity and Reynolds number, causing the coupling liquid to leave the laminar flow regime at a lower capacity flow ratio. The maximum effectiveness for each air flow rate with different numbers of liquid circuits are presented in Table 2. Maximum effectiveness increases with a reduction in the number of circuits.

For the case with one circuit presented in Fig. 11, it is obvious that the curves have different characteristics compared to Fig. 7. The change in effectiveness varies in a smoother manner with the capacity flow ratio and the maximum effectiveness is found at a capacity flow ratio close to unity for all air flow rates. In Appendix B, Figs. B1–B4 indicates how the number of circuits affects effectiveness with respect to the capacity flow ratio. An increase in the number of circuits results in an optimum effectiveness found at a capacity flow ratio beyond unity for certain air flow rates, because the transition out of the laminar flow regime is advanced.

## 4. Discussion

This study used correlations available in the open literature to find the convective heat transfer coefficients on the air side. Some of these correlations are developed for larger fin pitch and fewer tube rows than what is common in run-around heat recovery systems. To the best of the authors' knowledge, there is no correlation that includes and fits all the studied coils' parameters. An extrapolation out of the recommended range of applicability is performed for the correlation used to quantify air side performance. In order to verify that the correlations do not deviate to a large extent, the pressure drop was also modelled and compared to the measured pressure drop, presented in 2.2. Furthermore, several studies have shown that the effect of the fin pitch has a small to negligible effect on the Colburn factor and Fanning friction factor. Moreover, studies have also reported that the effect of the number of tube rows on the Colburn factor diminishes with an increased number of

tube rows, which thus motivates the extrapolation out of the recommended range. [32,35,36,37,38,39,40]

The modelling shows that the highest achievable effectiveness for the system drops with an increasing air flow rate due to lower NTU, these results corroborate the Holmberg [10] and Balen et al [14] findings. The coils' overall heat transfer coefficient U increases with an increased air and coupling liquid flow rate, i.e. higher fluid velocities that result in higher convective heat transfer coefficients. Nevertheless, an increase in the U-value of the coils does not always compensate for the higher capacity flow rate when the capacity flow ratio exceeds unity. This phenomenon is particularly pronounced for the case with 37% ethylene glycol presented in Fig. 6, where the maximum effectiveness for the air flow rate of 0.3 $m^3/s$ and 0.5 $m^3/s$ is found within the laminar flow regime on the liquid side. These results add new knowledge to the findings of Holmberg [10], Forsyth et al. [11,12] and Balen et al. [14], because maximum effectiveness is not always found for an operating condition resulting in turbulent flow on the liquid side.

For the case with an ethylene glycol concentration of 30 %, presented in Table 1 and in Figure A 3 (Appendix A), the maximum effectiveness achieved for the air flow rate of 0.7 $m^3/s$ was slightly higher than for $0.5 m^3/s$. The maximum effectiveness for the case with an air flow rate of $0.5 m^3/s$ is found after the transition out of the laminar flow regime, resulting in a capacity flow ratio of 1.42, compared to the case with an air flow rate of 0.7 $m^3/s$ where the maximum effectiveness was found at a capacity flow ratio of 1.14. The higher NTU for each individual coil operating with an air flow rate of $0.5 m^3/s$ does not compensate for the higher capacity flow ratio for the system, resulting in a slightly lower overall effectiveness.

While the increased Reynolds number on the liquid side reduces the heat transfer resistance in the coil, resulting in a higher UA-value for each individual coil presented in Fig. 8, the effectiveness for the system decreases due to the higher coupling liquid flow rate. Thus, there is an optimum capacity flow ratio, and increasing the coupling liquid flow rate further results in a reduced temperature difference $(T_{l,1} - T_{l,2})$ in Fig. 2, causing a reduction in heat transfer in each coil because the maximum temperature differences between the hot and the cold fluids are reduced.

Holmberg [10] assumed that the velocity was constant on the liquid side and Balen et al. [14] used pure water as the coupling liquid and concluded there is an optimum capacity flow ratio between the coupling liquid and air at unity. The modelling presented in this study show that there is not a single optimum capacity flow ratio independent of a) the air flow rate, b) the properties of the coupling liquid and c) the number of circuits. The results presented also add new knowledge to why Holmberg [10] and Balen et al. [14] found an optimum capacity flow ratio at unity. In the modelling using one circuit presented in Fig. 11, the coupling liquid leaves the laminar flow regime at a low capacity flow ratio, which is similar to the assumed constant velocity of Holmberg [10], which gives an optimum capacity flow ratio independent of air flow rate. Moreover, the same conclusion as Balen et al. [14] could be made for the cases modelled with low ethylene glycol concentrations presented in Fig. 9, because there is a shift towards finding an optimum capacity flow ratio close to unity. Forsyth et al. [12] analyzed data from field measurements in a system with a coupling liquid of 50% ethylene glycol and found that the optimum capacity flow ratio was higher than unity. The novelty of the present study is the analysis of how the optimum capacity flow ratio is affected by glycol concentration, air flow rate and number of circuits. This knowledge is crucial both when designing and operating run-around heat recovery systems, especially when designing systems for high thermal effectiveness.

The choice of glycol concentration is determined by the outdoor

climate. Two systems with the same coils used at different locations might have different characteristics of the effectiveness with regards to the capacity flow ratio. Due to the use of correlations to find the convective heat transfer coefficient and the Fanning friction factor for the air side, it is possible to use the presented model to perform parametric studies for different coil configurations. Since the effectiveness of a system will be higher with a higher coupling liquid flow velocity, there is a trade-off between the energy used for the pump and the recovered energy. The maximum velocity allowed on the liquid side is also dependent on the type of material used for the tubes to mitigate erosion, thus constraining the minimum number of circuits. Furthermore, there is a trade-off between fan energy and heat recovery, which depends on the desired supply air temperature, the climate where the system is installed and how the air flow varies between warmer and colder periods. This is particularly important for buildings using air to cool and to ventilate out internal heat gains, which could result in much higher air flow rates during warmer periods. Heat recovery could also take place during warmer periods if the extract air temperature is lower than the fresh supply air temperature, which must be accounted for when systems are optimized with regards to energy use, climate impact, operating costs and investment costs.

## 5. Conclusions

A model of a run-around heat recovery system using coils has been developed and verified using data from lab measurements. The model has been used to study how the system effectiveness is affected by air flow rate, coupling liquid flow rate, ethylene glycol concentration and the number of circuits. Using one liquid circuit or a low ethylene glycol concentration shows good agreement with previous reported findings, where the highest effectiveness is expected to be found at a capacity flow ratio of unity.

This study shows that maximum effectiveness is found at a capacity flow ratio of unity or higher than unity for all studied cases. The optimum coupling liquid flow rate can not be determined from just the air flow rate for all studied cases, coil configuration and ethylene glycol concentrations must be considered. For some operating conditions, the optimum capacity flow rate was found within the laminar flow regime on the liquid side.

Higher coupling liquid flow rates increase the UA-value of the coils, but on the other hand decrease the temperature difference of the coupling liquid, reducing the heat transfer in each coil, thus implying a trade-off for system effectiveness.

The presented model can be used to evaluate how other parameters besides the coupling liquid flow rate, the ethylene glycol concentration and circuiting, affect overall effectiveness. It is possible to use the model to study how different coil configurations affect the annual heat recovery and energy use for the fans and the pump.

## Declaration of Competing Interest

The authors declare that they have no known competing financial interests or personal relationships that could have appeared to influence the work reported in this paper.

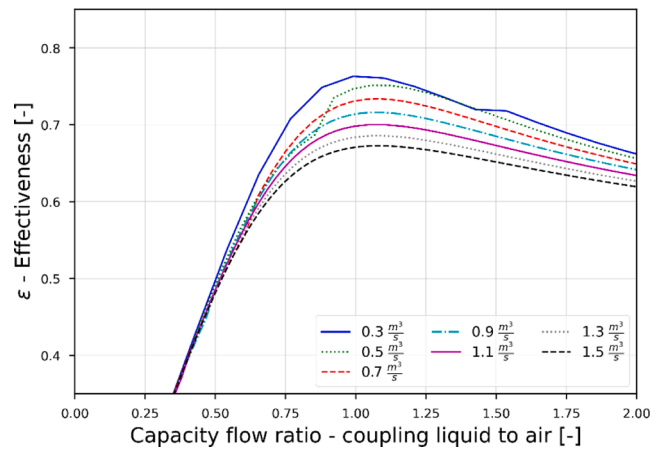## Appendix A:. Influence of glycol concentration

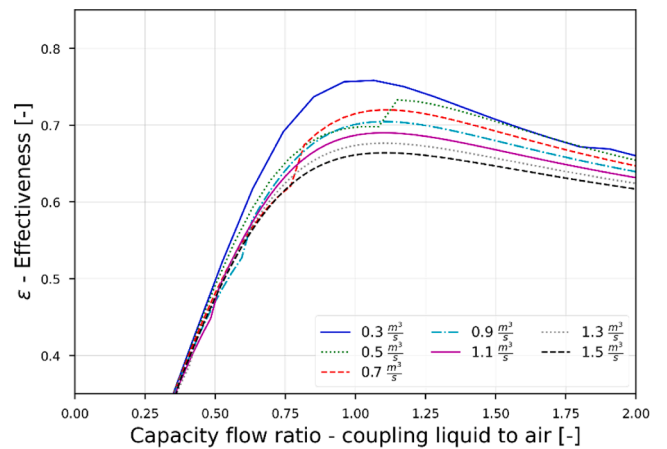See Figs. A1-A4.



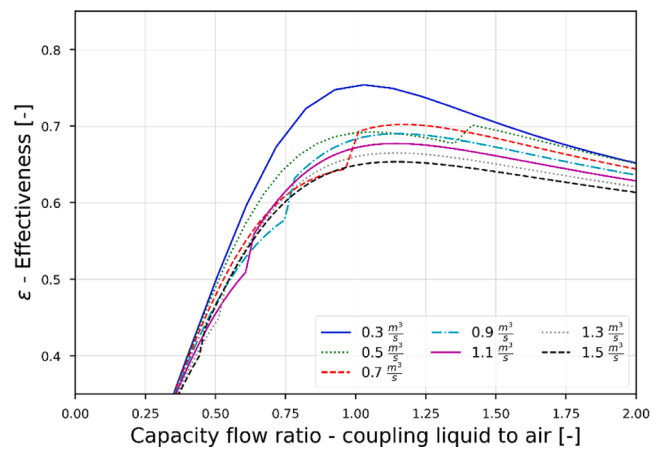**Fig. A1.** 10 % ethylene glycol.



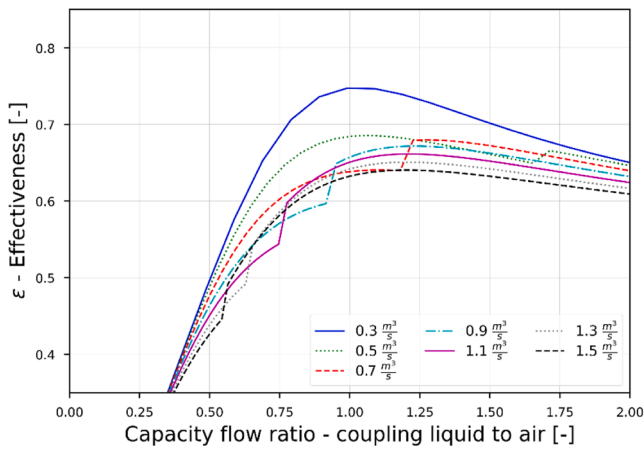**Fig. A2.** 20 % ethylene glycol.



**Fig. A3.** 30 % ethylene glycol.
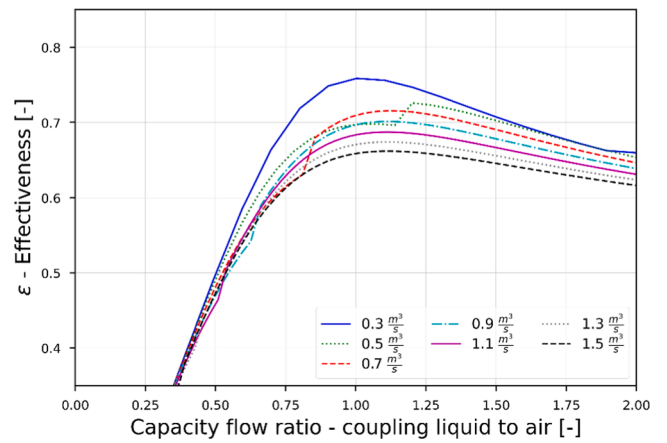
**Fig. A4.** 40 % ethylene glycol.

## Appendix B:. Influence of number of circuits

See Figs. B1-B4.



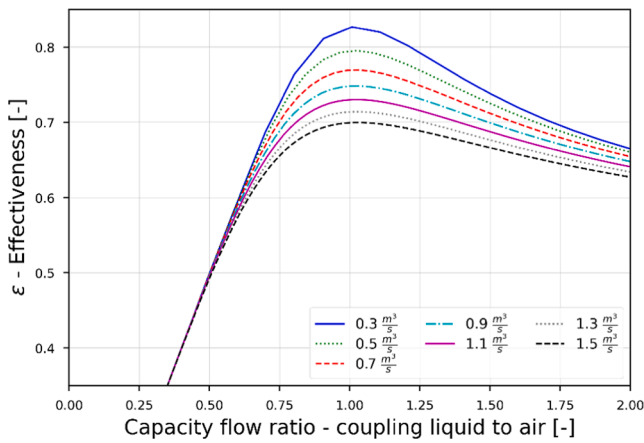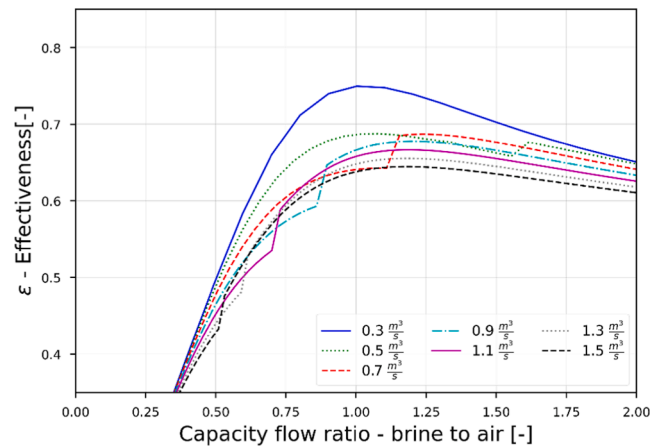**Fig. B1.** Using one circuit.



**Fig. B2.** Using two circuits.



**Fig. B3.** Using three circuits.



**Fig. B4.** Using four circuits.

## References

[1] IEA (2019), The Critical Role of Buildings, IEA, Paris https://www.iea.org/reports/the-critical-role-of-buildings.

[2] IEA (2020), Tracking Buildings 2020, IEA, Paris https://www.iea.org/reports/tracking-buildings-2020 accessed (2021-05-03).

[3] IEA (2020), Is cooling the future of heating?, IEA, Paris https://www.iea.org/commentaries/is-cooling-the-future-of-heating accessed (2021-05-03).

[4] IEA (2020), Energy Efficiency 2020, IEA, Paris https://www.iea.org/reports/energy-efficiency-2020 accessed (2021-05-03).

[5] REHVA COVID-19 guidance document, August 3, 2020.

[6] P. Filipsson, L. Ekberg "Vätskekopplad värmeåtervinning - Förstudie " CIT Energy Management, Göteborg, December, 2018.

[7] Commission Regulation (EU) No 1253/2014 of July 2014 implementing Directive 2009/125/EC of the European Parliament and of the Council with regard to ecodesign requirements for ventilation units.

[8] A. Mardiana-Idayu, S.B. Riffat, Review on heat recovery technologies for building applications, Renewable and Sustainable Energy Reviews 16 (2) (2012) 1241–1255.

[9] W.M. Kays, and A.L. London, "Compact heat exchangers", United States, 1984.

[10] R.B. Holmberg, Heat Transfer in Liquid-Coupled Indirect Heat Exchanger Systems, ASME J. Heat Transfer. 97 (4) (November 1975) 499–503.

[11] B.I. Forsyth, R.W. Besant, The design of a run-around heat recovery system, ASHRAE transactions. 94 (1988) 511–531.

[12] B.I. Forsyth, R.W. Besant, The performance of a run-around heat recovery system using aqueous glycol as coupling liquid, ASHRAE transactions. 94 (1988) 532–545.

[13] Y.Y. Zeng, R.W. Besant, K.S. Rezkallah, The effect of temperature-dependent properties on the performance of run-around heat recovery systems using aqueous-glycol coupling fluids, ASHRAE Trans. 98 (l) (1992) 551–562.

[14] I. Balen, P. Donjerkovic, I. Galaso, Analysis of the coil energy recovery loop system, Int. J. Energy Res. 27 (4) (2003) 363–376.

[15] H. Fan, R.W. Besant, C.J. Simonson, W. Shang, Run-Around Heat Recovery System Using Cross-Flow Flat-Plate Heat Exchangers with Aqueous Ethylene Glycol as the Coupling Fluid, ASHRAE Transactions 111 (1) (2005) 901–910.

[16] Alireza Vali, Carey J. Simonson, Robert W. Besant, Gazi Mahmood, Numerical model and effectiveness correlations for a run-around heat recovery system with combined counter and cross flow exchangers, International Journal of Heat and Mass Transfer 52 (25-26) (2009) 5827–5840.

[17] Jörgen Wallin, Hatef Madani, Joachim Claesson, Run-around coil ventilation heat recovery system: A comparative study between different system configurations, Applied Energy 90 (1) (2012) 258–265.

[18] F.P. Incropera, D.P. DeWitt, T.L. Bergman, A.S. Lavine, Principles of Heat and Mass Transfer, 7th ed., Wiley & Sons, New York, 2013.

[19] T. Sun, A. S. Teja, "Density, Viscosity, and Thermal Conductivity of Aqueous Ethylene, Diethylene, and Triethylene Glycol Mixtures between 290 K and 450 K"Journal of Chemical & Engineering Data 2003 48 (1), pp. 198-202.

[20] P. Giacomo, "Equation for the Determination of the Density of Moist Air" 1982 Metrologia 18 33.

[21] Changsheng Yang, Peisheng Ma, Fengming Jing, Duoqiang Tang, Excess Molar Volumes, Viscosities, and Heat Capacities for the Mixtures of Ethylene Glycol + Water from 273.15 K to 353.15 K, Journal of Chemical & Engineering Data 48 (4) (2003) 836–840.

[22] N.G. Kingman, A. Rosenberg, M. Bastos, I. Wadsö, Heat capacity of poly(ethylene glycol)-water mixtures: poly(ethylene glycol)-water interactions, Thermochimica Acta 169 (1990) 339–346.

[23] D. Bohne, S. Fischer, E. Obermeier, Thermal, Conductivity, Density, Viscosity, and Prandtl-Numbers of Ethylene Glycol-Water Mixtures, Berichte der Bunsengesellschaft für physikalische Chemie 88 (8) (1984) 739–742.

[24] P.T. Tsilingiris, Thermophysical and transport properties of humid air at temperature range between 0 and 100°C, Energy Conversion and Management 49 (5) (2008) 1098–1110.

[25] W. Afzal, A. H. Mohammadi, D. Richon, "Volumetric Properties of Mono-, Di-, Tri-, and Polyethylene Glycol Aqueous Solutions from (273.15 to 363.15) K: Experimental Measurements and Correlations" J. Chem. Eng. Data 2009, 54, 4, pp 1254–1261.

[26] S. M. Ghiassiaan, "Convective Heat and Mass Transfer", 2nd ed, 2018.

[27] P.S. Hrnjak, S.H. Hong, "Effect of Return Bend and Entrance on Heat Transfer in Thermally Developing Laminar Flow in Round Pipes of Some Heat Transfer Fluids With High Prandtl Numbers." ASME. J. Heat Transfer. June 2010; 132(6): 061701.

[28] Caroline Haglund Stignor, Bengt Sundén, Per Fahlén, Liquid side heat transfer and pressure drop in finned-tube cooling-coils operated with secondary refrigerants, International Journal of Refrigeration 30 (7) (2007) 1278–1289.

[29] Chi-Chuan Wang, Investigation of wavy fin-and-tube heat exchangers: a contribution to databank, Experimental Heat Transfer 12 (1) (1999) 73–89.

[30] R.K. Shah, D.P. Sekulic, "Fundamentals of Heat Exchanger Design" Wiley, New Jersey (2003).

[31] Th.E. Schmidt, "Heat transfer calculations for extended surfaces" Refrigerating Engineering, April (1949), pp. 351–357.

[32] C.C. Wang, "On the Airside Performance of Fin-and-Tube Heat Exchangers." In: Kakaç S., Bergles A.E., Mayinger F., Yüncü H. (eds) Heat Transfer Enhancement of Heat Exchangers. Nato ASI Series (Series E: Applied Sciences), vol 355. Springer, Dordrecht.

[33] L.H. Tang, Z. Min, G.N. Xie, Q.W. Wang, "Fin Pattern Effects on Air-Side Heat Transfer and Friction Characteristics of Fin-and-Tube Heat Exchangers with Large Number of Large-Diameter Tube Rows" Heat Transfer Engineering, 30:3, pp. 171-180, 2009.

[34] Y.B. Tao, Y.L. He, J. Huang, Z.G. Wu, W.Q. Tao, "Numerical study of local heat transfer coefficient and fin efficiency of wavy fin-and-tube heat exchangers" International Journal of Thermal Sciences, Volume 46, Issue 8, 2007, pp. 768-778,.

[35] B. Youn, N.H. Kim, "An experimental investigation on the airside performance of fin-and-tube heat exchangers having sinusoidal wave fins." Heat Mass Transfer 43, pp. 1249–1262 (2007).

[36] Chi-Chuan Wang, Yu-Juei Chang, Yi-Chung Hsieh, Y.T. Lin, "Sensible heat and friction characteristics of plate fin-and-tube heat exchangers having plane fins"International, Journal of Refrigeration 19 (4) (1996) 223–230.

[37] A.H. Elmahdy, R.C. Biggs, "Finned tube heat exchanger: Correlation of dry surface heat transfer data"A.S.H.R.A.E. TRANS.; USA; DA. 1979; Vol. 85; no 2; pp. 262-273; Bibl. 22.

[38] D.G. Rich, "The effect of fin spacing on the heat transfer and friction performance of multi-row, smooth plate fin-and-tube heat exchangers" A.S.H.R.A.E. TRANS.; U. S.A.; DA. 1973; Vol. 79; part. 2; pp. 137-145; Bibl. 9.

[39] Somchai Wongwises, Yutasak Chokeman, Effect of fin pitch and number of tube rows on the air side performance of herringbone wavy fin and tube heat exchangers, Energy Conversion and Management 46 (13-14) (2005) 2216–2231.

[40] Y.C. Liu, I.Y. Chen, R. Hu, C.C. Wang, B.C Yang "Sensible Airside Performance of Fin-and-Tube Heat Exchangers-Data with Larger Diameter Tube", ASHRAE Transactions; Atlanta 114 (2008) 379–386.